Asian Journal of Chemistry; Vol. 37, No. 5 (2025), 1049-1059

ASIAN JOURNAL OF CHEMISTRY

https://doi.org/10.14233/ajchem.2025.33493

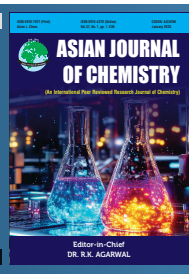

Synthesis, Biological Evaluation and Molecular Modelling Studies of Thiophene Piperazine-Carbamate Derivatives as Multi-Target Agents for Alzheimer's Disease

Bala Yesu Valaparla[1,2], Yelamanda Rao Kandrakonda[3], Sajitha Kethineni[1], Vamsi Katta[4], Suresh Babu Donka[1], Manjunadh D. Meti[5], Uttam A. More[6], A.G. Damu[3] and Srinivasulu Doddaga[1,*]

[1]Department of Chemistry, Sri Venkateswara University, Tirupati-517502, India
[2]Department of Chemistry, SGK Government Degree College, Vinukonda, Palnadu-522647, India
[3]Bioorganic Chemistry Research Laboratory, Department of Chemistry, Yogi Vemana University, Kadapa-516005, India
[4]Indian Institute of Science Education and Research (IISER), Tirupati-517507, India
[5]Department of Plant Sciences, School of Life Sciences, University of Hyderabad, Gachibowli-500046, India
[6]Department of Pharmaceutical Chemistry, Shree Dhanvantary Pharmacy College, Kim, Suram-394110, India

*Corresponding author: E-mail: doddaga_s@yahoo.com

Received: 10 February 2025; *Accepted*: 19 March 2025; *Published online*: 30 April 2025; AJC-21969

Alzheimer's disease is a progressive neurodegenerative condition marked by cognitive deterioration, memory deficits and behavioural changes, underscoring the pressing need for innovative therapeutic strategies. While acetylcholinesterase (AChE) inhibitors remain a cornerstone in managing cholinergic dysfunction in AD, the multifaceted nature of the disease, which also involves oxidative stress, necessitates the development of multi-targeted therapeutic agents. In response to this challenge, a series of novel thiophene piperazine-carbamate hybrids (**8a-g**) was designed and synthesized to simultaneously inhibit AChE and butyrylcholinesterase (BChE), while also possessing potent antioxidant properties, as evidenced by ABTS radical scavenging activity. *In vitro* analysis revealed robust inhibition of AChE and BChE across all compounds, with a clear preference for AChE inhibition. Among these hybrids, compound **8e** exhibited exceptional potency, achieving AChE inhibition (IC_{50} = 0.12 ± 0.001 µM), BChE inhibition (IC_{50} = 12.29 ± 0.02 µM) and antioxidant activity (IC_{50} = 0.192 ± 0.001 µM). Biophysical kinetic studies confirmed that compound **8e** operates *via* mixed-type inhibition of AChE, with inhibition constants (K_{i1} = 0.158 µM, K_{i2} = 0.347 µM). Molecular docking studies substantiated that both compounds bind effectively to key residues in the catalytic active site (CAS) and peripheral anionic site (PAS) of AChE, supporting their dual inhibition mechanism. Significantly, compounds **8e**, **8d**, **8g** and **8a** stand out as promising candidates for further development due to their dual-target inhibition and antioxidant properties. Structure-activity relationship (SAR) analysis highlighted that shorter, unbranched alkyl chains enhance binding affinity and inhibitory potency, while bulkier or branched groups introduce steric hindrance, reducing efficacy. Collectively, these findings position the thiophene piperazine-carbamate hybrids, particularly compounds **8e** and **8d**, as potent multi-target agents with significant potential for addressing both cholinergic dysfunction and oxidative stress in Alzheimer's disease therapy.

Keywords: Thiophene, Piperazine, Carbamates, Alzheimer, Acetylcholinesterase, Butyrylcholinesterase, Molecular docking.

INTRODUCTION

Alzheimer's disease (AD) is the leading cause of dementia globally, presenting a significant health, social and economic burden. The disease typically starts with memory loss and progresses to cognitive impairments, including difficulties with visuospatial skills, navigation and executive function. As it advances, individuals experience greater challenges in daily activities, severely affecting quality of life. In the later stages, behavioural and psychological symptoms such as depression, anxiety, hallucinations and sleep disturbances become more prominent. Comorbidities like hypertension, diabetes and cardiovascular disease can accelerate cognitive decline. In the most advanced stages, complications such as mobility impairments, dysphagia, malnutrition and pneumonia are common, increasing mortality risk and further compromising the patient's well-being [1,2]. The global prevalence of AD is staggering, with over 55.2 million people affected worldwide. Projections

suggest this number could rise to 82 million by 2030 and 139 million by 2050, highlighting the urgent need for more effective treatments to address this growing public health crisis [3].

The pathophysiology of AD is multifactorial, involving genetic, environmental and aging-related factors. Central to the disease are cholinergic dysfunction, the accumulation of amyloid-β (Aβ) plaques, neurofibrillary tangles (NFTs), neuroinflammation and oxidative stress, which drive cognitive decline and neuronal damage. Metal ion imbalances and mitochondrial dysfunction further exacerbate these processes, leading to ther synaptic failure and neuronal loss. However, the exact causes of these pathological changes remain unclear, making AD difficult to treat effectively. The enzymes acetylcholinesterase (AChE) and butyrylcholinesterase (BChE) are responsible for the breakdown of ACh in the brain. Inhibiting these enzymes to reduce ACh hydrolysis is a corner-stone of current therapeutic strategies for AD. AChE inhibitors such as donepezil, galantamine and rivastigmine are widely used to increase ACh levels, thereby improving neurotransmission and alleviating cognitive symptoms [4]. Recently, BChE has also emerged as an important target, as it plays a role in regulating ACh levels and even modulating amyloid-β release. This highlights the potential benefit of dual inhibition of both AChE and BChE in AD treatment [5,6].

Another critical area in AD pathogenesis is the oxidative stress. The overproduction of reactive oxygen species (ROS) and the decline in cellular antioxidant defenses contribute to neuronal damage, synaptic dysfunction and cognitive impairment. Oxidative stress exacerbates amyloid-β plaque formation, tau hyperphosphorylation and neuronal degeneration. Thus, combining cholinesterase inhibition with antioxidant activity offers a promising therapeutic approach to mitigate both cholinergic dysfunction and oxidative damage in AD [7,8].

AD is a multifactorial disorder, which makes finding a single, effective treatment particularly challenging. Multi-target-directed ligands (MTDLs) present a promising strategy, as they can simultaneously modulate multiple pathological targets involved in neurodegenerative diseases. MTDLs are typically synthesized by connecting the pharmacophores of various ligands, often incorporating small organic molecules and heterocyclic compounds known for their favourable physicochemical properties and ability to inhibit enzymes [9]. Particularly, thiophene derivatives are valuable in drug design due to their broad pharmacological activity, including antipsychotic, antianxiety, antimicrobial, anti-inflammatory and antioxidant effects. Their structural diversity and ability to form key interactions with biological targets especially *via* sulphur-based hydrogen bonding make them potent candidates [10]. Additionally, piperazine, a six-membered nitrogen-containing heterocycle, has emerged as a critical component in rational drug design. It is found in a wide range of well-known therapeutic agents, such as antipsychotics, antihistamines, antianginals, antidepressants, anticancer drugs and more [11]. Minor structural modifications to piperazine can significantly alter the medicinal potential of resulting molecules, which enhances its appeal in drug development for diseases like AD [12]. When combined with thiophene, piperazine improves the pharmacological profile of drugs, offering synergistic effects such as anti-inflammatory, anticancer, antiviral, antimicrobial and anti-alzheimer properties [13,14]. The combination of these two moieties (Fig. 1) allows for an integrated approach to target multiple AD-related pathways, including cholinergic dysfunction, oxidative stress and neuroinflammation, as suggested by recent studies [15].

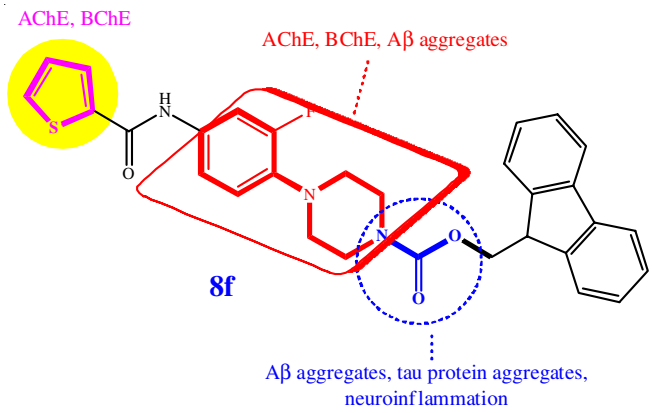

Fig. 1. Core-linker-base architecture of thiophene piperazine-carbamate hybrids

Furthermore, the carbamate moiety, known for its ability to enhance chemical stability, metabolic stability and bioavailability, plays a critical role in drug design. Carbamate-based compounds have demonstrated significant therapeutic efficacy in a range of disorders, including AD, cancer and infectious diseases [16]. Notably, rivastigmine, a carbamate-based drug, is an established inhibitor of acetylcholinesterase and has been used to treat AD [17,18]. Leveraging these structural principles, our research focuses on developing novel thiophene piperazine-carbamate derivatives designed to inhibit both AChE and BChE, which are pivotal enzymes in AD pathophysiology. These compounds also aim to provide antioxidant and anti-inflammatory effects, further targeting the complex and multifactorial nature of AD. We conducted molecular docking studies to assess the interaction profiles of these compounds with AChE, BChE and antioxidant targets, providing valuable insights into their mechanisms of action and guiding the refinement of these compounds for improved therapeutic potential [19]. By integrating these multi-target strategies, we aim to develop more effective agents capable of addressing the diverse pathological aspects of AD, ultimately improving therapeutic outcomes for patients, as supported by recent advances in the field.

EXPERIMENTAL

All chemicals were procured from Merck, TCI, Sigma Aldrich, Avra and used without purification. All the procedures and biological experiments were carried out by using double deionized water. The TLC plates with 0.25 mm and an iodine chamber or UV lamp (254 nm) visualization were utilized for monitoring all reactions. As per requirement, compoun were purified using column chromatography with silica gel (60–120 mesh). On Shimadzu-8400 spectrometer IR spectra were

recorded KBr pellet. ^{1}H NMR and ^{13}C NMR spectra were measured at 400 MHz and 100 MHz on a Bruker spectrometer with $CDCl_3$/DMSO-d_6 solvents and TMS as an internal standard for intermediates and target compounds. The mass spectrometer Xevo TQD Quadrupole (QCA583) was used to measure HR-MS.

General synthesis of thiophene piperazine carbamate hybrids (8a-g)

General procedure of synthesis of 3,4-difluoronitrobenzene (1): *o*-Difluoro benzene (0.39 mmol) was nitrated by dropwise addition of a mixture of conc. HNO_3 and conc. H_2SO_4 over 2 h at 10-15 ºC with continuous stirring. After the addition, the reaction mixture was stirred at 45-50 ºC for 4 h. The reaction was then quenched by pouring it into ice water. The organic phase was separated and the aqueous phase was extracted with $CHCl_3$ (3 × 50 mL). The combined organic extracts were washed with water (3 × 50 mL) and dried over anhydrous Na_2SO_4. The organic layer was concentrated under vacuum and distilled to obtained residue **1**.

Synthesis of 1-(2-fluoro-4-nitro-phenyl)piperazine (2): A mixture of 3,4-difluoronitrobenzene (**1**, 7.5 mmol) in 50 mL of acetonitrile was mixed with piperazine (18.8 mmol) and heated under reflux for 3 h. After cooling to room temperature, the mixture was concentrated *in vacuo*. The residue was then diluted with water and extracted with EtOAc (3 × 50 mL) and satd. NH_4Cl (2 × 50 mL) solution, then dried over anhydrous Na_2SO_4. The solvent was removed under vacuum and purified by column chromatography to obtain compound **2**.

Synthesis of *tert*-butyl 4-(2-fluoro-4-nitrophenyl)piperazine-1-carboxylate (3): To a solution of piperazinyl compound (**2**, 3.2 mmol) in THF (20 mL), di-*tert*-butyl dicarbonate (3.78 mmol), a satd. solution of $NaHCO_3$ (15 mL) and Milli-Q water (15 mL) were added sequentially. The mixture was stirred at 25 ºC for 5 h, then extracted twice with CH_2Cl_2. The combined organic layers were washed with brine, dried over anhydrous Na_2SO_4. The solvent was removed under vacuum and purified by using column chromatography led to the formation of compound **3** as a deep yellow powder.

Synthesis of *tert*-butyl 4-(4-amino-2-fluorophenyl) piperazine-1-carboxylate (4): To a solution of compound **3** (6.15 mmol) in THF and CH_3OH, cooled to below 5 ºC, a saturated solution of $CuSO_4$ (27 mL) was added. The resulting mixture was stirred vigorously and $NaBH_4$ (107 mmol) was added in portions. The mixture was then filtered through celite and the filtrate was subsequently diluted with 200 mL of Milli-Q water and 400 mL of CH_2Cl_2. After the separation of organic phase which was extracted twice with CH_2Cl_2. The combined organic extracts were washed with brine, dried over anhydrous Na_2SO_4 and filtered. The solvent was removed under reduced pressure, yielding a brownish oily residue of the desired amine **4**.

Synthesis of *tert*-butyl 4-(2-fluoro-4-(thiophene-2-carboxamido)phenyl)piperazine-1-carboxylate (5): To an ice-cooled solution of compound **4** (10 mmol) in 5 mL of DMF, thiophene-2-carboxylic acid (12 mmol), hydroxy benzotriazole (HOBt, 15 mmol), (3-dimethylaminopropyl)ethylcarbodiimide hydrochloride (EDC·HCl, 20 mmol) and a few drops of N,N-diisopropylethylamine (DIPEA) were added. The mixture was stirred at room temperature for 1 h. Subsequently, the reaction mixture was poured onto crushed ice. The resulting precipitate was filtered, dried and recrystallized from ethanol to yield compound **5**.

Synthesis of *N*-(3-fluoro-4-(piperazin-1-yl)phenyl)thiophene-2-carboxamide (6): Compound **5** (10 mmol) and TFA (20 mmol) was suspended in 20 mL of DCM at ambient temperature and stirred for 2 h. After completion of the reaction, the crude was concentrated under reduced pressure. The compound was dissolved in 5 mL of water, saturated Na_2CO_3 solution was used to adjust the pH 8-9. The aqueous layer was extracted with DCM (3 × 10 mL) and organic layer was washed with satd. $NaHCO_3$, brine followed by water. Then dried over with anhydrous Na_2SO_4. The organic layer was concentrated under vacuum and purified by using column chromatography to yield compound **6** as a pale yellow solid.

General procedure of synthesis of carbamates of *N*-(3-fluoro-4-(piperazin-1-yl)phenyl)thiophen-2-amine hybrids (8a-g): To a solution of **6**, (1.1 mmol), triethylamine (1.3 mmol) and various substituted chloroformates **7a-g**, (2.2 mmol) in 5 mL THF, was added dropwise over a period of 20 min. After stirring the mixture at 40 ºC for 2 h, it was poured into 10 mL of water. The solution was neutralized with 1N HCl and the resulting precipitate was filtered and washed with water (**Scheme-I**). The crude product was dried in a vacuum desiccator and further purified by column chromatography to yield **8a-g** as solids.

Pentyl-4-(2-fluoro-4-(thiophene-2-carboxamido)-phenyl)piperazine-1-carboxylate (8a): Pale green solid, yield: 68%; m.p.: 168-172 ºC; FT-IR (KBr, ν_{max}, cm^{-1}): 3325, 2943, 2830, 1738, 1654, 1424, 1114, 1022; ^{1}H NMR ($CDCl_3$, 400 MHz) δ ppm: 9.54 (s, 1H), 7.80 (m, 1H), 7.59-7.55 (m, 1H), 7.48-7.46 (m, 1H), 7.36-7.33 (m, 2H), 7.04 (m, 1H), 6.85-6.81 (m, 1H), 4.04-4.01 (t, 2H), 3.57 (m, 4H), 2.94 (m, 4H), 1.60-1.57 (m, 2H), 1.33-1.22 (m, 4H), 0.87-0.83 (t, 3H); ^{13}C NMR ($CDCl_3$, 100 MHz) δ ppm: 160.30, 156.41, 155.43, 154.82, 140.11, 135.87, 134.11, 130.71, 128.64, 119.02, 116.24, 109.34, 65.53, 50.40, 49.68, 28.56, 27.99, 22.22, 13.91; m.f.: $C_{21}H_{28}FN_3O_3S$; calcd. m.w.: 419.52: HRMS: 420.1754 $[M+H]^+$.

***tert*-Butyl-4-(2-fluoro-4-(thiophene-2-carboxamido)-phenyl)piperazine-1-carboxylate (8b):** Pale yellow solid, yield: 73%; m.p.: 171-175 ºC; FT-IR (KBr, ν_{max}, cm^{-1}) : 3314, 2943, 2831, 1738, 1654, 1448, 1216, 1022; ^{1}H NMR ($CDCl_3$, 400 MHz) δ ppm: 9.64 (s, 1H), 7.81 (m, 1H), 7.60-7.56 (m, 1H), 7.48 (m, 1H), 7.36-7.33 (m, 1H), 7.04 (m, 1H), 6.86-6.81 (m, 1H), 3.57-3.54 (m, 4H), 2.95 (m, 4H), 0.89-0.87 (d, 9H); ^{13}C NMR ($CDCl_3$, 100 MHz) δ ppm: 160.29, 153.17, 152.88, 140.17, 135.44, 134.37, 130.72, 128.66, 127.48, 119.07, 116.24, 109.32, 79.34, 50.40, 49.68, 28.39; m.f.: $C_{20}H_{24}FN_3O_3S$; calcd. m.w.: 405.49: HRMS: 406.1597 $[M+H]^+$.

Isobutyl-4-(2-fluoro-4-(thiophene-2-carboxamido)-phenyl)piperazine-1-carboxylate (8c): Off-white solid, yield: 74%; m.p.: 171-175 ºC; FT-IR (KBr, ν_{max}, cm^{-1}) : 3321, 2944, 2831, 1738, 1695, 1448, 1216, 1114, 1022; ^{1}H NMR ($CDCl_3$, 400 MHz) δ ppm: 9.61 (s, 1H), 7.81 (m, 1H), 7.60-7.57 (m, 1H), 7.48-7.46 (m, 1H), 7.38-7.34 (m, 2H), 7.05-7.01 (m, 1H),

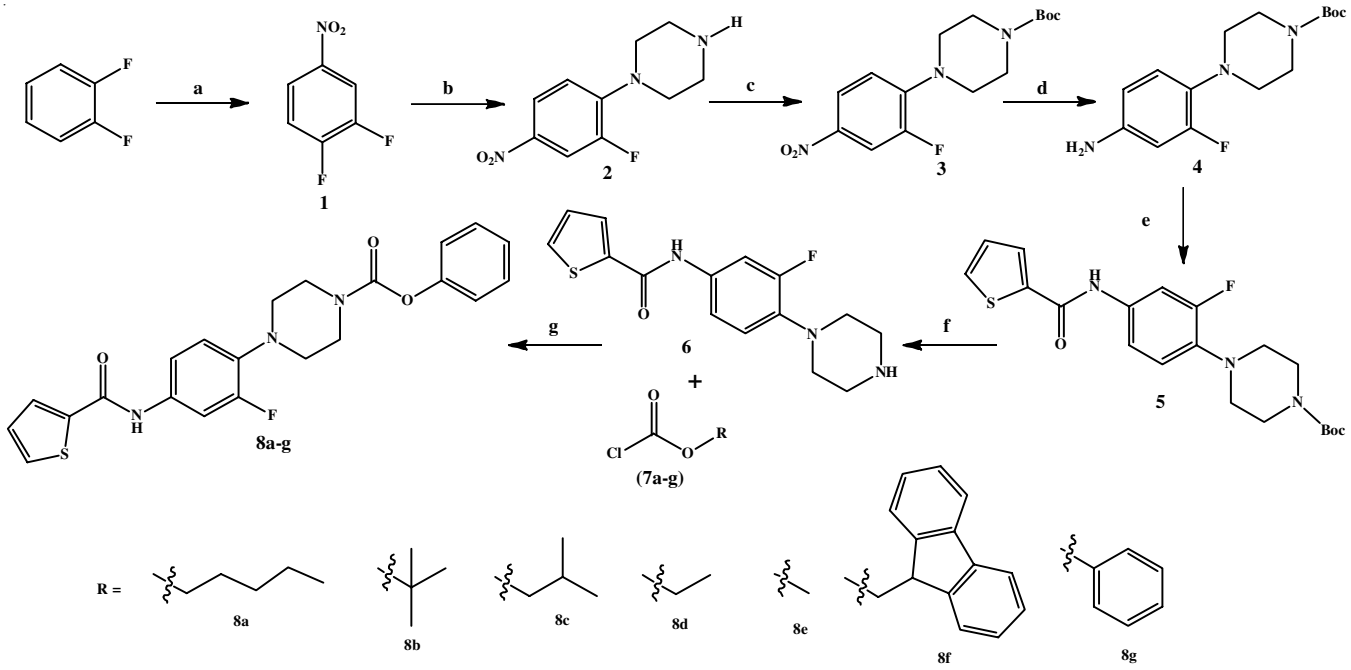

Scheme-I: Synthesis of thiophene piperazine-carbamate hybrids (**8a-g**) [Reagents and conditions: (a) HNO_3, H_2SO_4, 45 ºC; (b) piperazine, CH_3CN, 80 ºC; (c) Boc_2O, THF, 25 ºC; (d) $CuSO_4$, THF, $NaBH_4$, CH_3OH, 5 ºC; (e) EDC·HCl, HOBt, DIPEA, DMF; (f) TFA, DCM; g. TEA, THF]

6.85-6.81 (m, 1H), 3.82-3.80 (t, 2H), 3.69-3.56 (m, 4H), 2.99-2.94 (m, 4H), 0.98-0.96 (d, 6H); ^{13}C NMR ($CDCl_3$, 100 MHz) δ ppm: 161.22, 156.39, 154.82, 140.10, 134.51, 134.39, 133.72, 129.79, 128.39, 119.76, 119.73, 118.01, 109.76, 79.34, 50.40, 49.68, 28.39, 18.99; m.f.: $C_{20}H_{24}FN_3O_3S$; calcd. m.w.: 405.49: HRMS: 406.1597 $[M+H]^+$.

Ethyl-4-(2-fluoro-4-(thiophene-2-carboxamido)phenyl)-piperazine-1-carboxylate (8d): Off-white solid, yield: 69%; m.p.: 171-175 ºC; FT-IR (KBr, ν_{max}, cm^{-1}) : 3325, 2944, 2831, 1701, 1695, 1590, 1446, 1216, 1022; ^{1}H NMR ($CDCl_3$, 400 MHz) δ ppm: 9.62 (s, 1H), 7.81-7.79 (m, 1H), 7.59-7.54 (m, 1H), 7.48-7.45 (m, 1H), 7.40-7.33 (m, 2H), 7.05-7.01 (m, 1H), 6.85-6.79 (m, 1H), 4.09-4.06 (t, 2H), 3.57-3.54 (m, 4H), 2.95-2.92 (m, 4H), 1.21-1.19 (t, 3H); ^{13}C NMR ($CDCl_3$, 100 MHz) δ ppm: 160.27, 156.33, 153.89, 140.11, 135.70, 134.23, 130.17, 128.63, 127.47, 118.98, 116.22, 109.29, 71.74, 50.40, 49.68, 13.91; m.f.: $C_{18}H_{20}FN_3O_3S$; calcd. m.w.: 377.43; HRMS: 400.1100 $[M+Na]^+$.

Methyl-4-(2-fluoro-4-(thiophene-2-carboxamido)-phenyl)piperazine-1-carboxylate (8e): Off-white solid, yield: 66%; m.p.: 184-188 ºC; FT-IR (KBr, ν_{max}, cm^{-1}) : 3314, 2943, 2831, 1738, 1695, 1449, 1420, 1216, 1022; ^{1}H NMR ($CDCl_3$, 400 MHz) δ ppm: 9.54 (s, 1H), 7.87-7.79 (m, 1H), 7.59-7.55 (m, 1H), 7.48-7.46 (m, 1H), 7.36-7.33 (m, 2H), 7.05-7.01 (m, 1H), 6.85-6.79 (m, 1H), 4.04-4.01 (t, 2H), 3.57-3.54 (m, 4H), 2.95-2.92 (m, 4H), 1.60-1.57 (m, 2H), 1.33-1.22 (m, 4H), 0.87-0.83 (t, 3H); ^{13}C NMR ($CDCl_3$, 100 MHz) δ ppm: 160.27, 154.82, 151.90, 140.10, 130.72, 129.46, 158.63, 127.47, 125.19, 121.62, 119.76, 117.95, 109.76, 50.40, 49.68, 49.65; m.f.: $C_{17}H_{18}N_3FO_3S$; calcd. m.w.: 363.41; HRMS: 364.1116 $[M+H]^+$.

(9*H*-Fluoren-9-yl)methyl-4-(2-fluoro-4-(thiophene-2-carboxamido)phenyl)piperazine-1-carboxylate (8f): Off-white solid, yield: 72%; m.p.: 182-186 ºC; FT-IR (KBr, ν_{max}, cm^{-1}) : 3314, 2943, 2831, 1737, 1695, 1448, 1216, 1022; ^{1}H NMR ($CDCl_3$, 400 MHz) δ ppm: 9.68 (s, 1H), 7.82-7.79 (m, 1H), 7.68-7.66 (m, 2H), 7.60-7.46 (m, 5H), 7.41-7.20 (m, 6H), 7.02-7.01 (m, 1H), 6.81 (m, 1H), 4.37 (d, 2H), 3.83 (m, 1H), 3.54 (m, 4H), 2.89 (m, 4H); ^{13}C NMR ($CDCl_3$, 100 MHz) δ ppm: 160.30, 154.91, 144.99, 143.77, 141.09, 140.09, 135.58, 134.29, 130.73, 128.67, 127.61, 127.13, 126.98, 126.73, 125.00, 124.82, 119.85, 119.01, 116.24, 109.29, 67.09 50.42, 49.68, 47.15; m.f.: $C_{30}H_{26}FN_3O_3S$; calcd. m.w.: 527.61; HRMS: 528.1920 $[M+H]^+$.

Phenyl-4-(2-fluoro-4-(thiophene-2-carboxamido)-phenyl)piperazine-1-carboxylate (8g): Off-white solid, yield: 74%; m.p.: 185-189 ºC; FT-IR (KBr, ν_{max}, cm^{-1}) : 3316, 2942, 2831, 1738, 1695, 1448, 1216, 1022; ^{1}H NMR ($CDCl_3$, 400 MHz) δ ppm: 9.54 (s, 1H), 7.87-7.79 (m, 1H), 7.59-7.55 (m, 1H), 7.48-7.46 (m, 1H), 7.36-7.33 (m, 2H), 7.05-7.01 (m, 1H), 6.85-6.79 (m, 1H), 4.04-4.01 (t, 2H), 3.57-3.54 (m, 4H), 2.95-2.92 (m, 4H), 1.60-1.57 (m, 2H), 1.33-1.22 (m, 4H), 0.87-0.83 (t, 3H); ^{13}C NMR ($CDCl_3$, 100 MHz) δ ppm: 161.22, 156.39, 154.82, 144.99, 140.10, 134.51, 134.39, 133.72, 133.63, 132.35, 129.79, 128.39, 119.76, 119.73, 118.01, 117.95, 109.76, 50.42, 49.68; m.f.: $C_{22}H_{20}FN_3O_3S$; calcd. m.w.: 425.48; HRMS: 448.1100 $[M+Na]^+$.

In vitro biological assays

Cholinesterase inhibitory activity assay: Elmann's spectrophotometric method was used to assess cholinesterase (AChE & BChE) inhibitory activity using EeAChE (*Electrophorus electricus*) and EqBChE (from horse serum) with some modifications [20]. Phosphate buffer solution (pH = 7.7, 200 mM) was freshly prepared for assay. Test sample solutions (1 mM)

were prepared by dissolving target compounds in appropriate amount of DMSO and diluted with phosphate buffer solution (pH = 7.7, 200 mM) to yield final concentration range. In a 96-well microplate, the following were added in order of 145 µL phosphate buffer solution, 10 µL test compounds solution, 80 µL 5,5-dithio-*bis*-(2-nitrobenzoic acid) (DTNB) solution (18.5 mg in 10 mL phosphate buffer solution) and 10 µL AChE or BChE solution (4 mU/mL enzyme in 10 mL phosphate buffer). To the assay mixture, added 15 µL of 1 mM acetylthiocholine/butyrylthiocholine (ATCh/BTCh) substrate and assayed after 5 min of pre-incubation at 25 ºC using Elisa microplate reader (Bio-Rad) at 415 nm absorbance. Galantamine was a reference drug using the same technique. Control tests were done with the reaction mixture without test sample. The calculation of the inhibition percentage was performed using the equation $(1\text{-}A_{bst}/A_{bsc}) \times 100$, where A_{bst} and A_{bsc} denote the absorbance values of AChE in the presence and absence of the test compounds, respectively. The IC_{50} values were determined using interpolation from linear regression analysis and are reported as the mean ± standard error of the mean (SEM) [21].

Kinetics study of AChE inhibition: AChE inhibition by the most potent analogue **8e** was kinetically assessed using Ellman's method to calculate the inhibition constant K_i and understand the type of inhibition. Inhibitor, substrate, enzyme and DTNB stock solutions were prepared in phosphate buffer solution (pH 7.7) 2, 2.5 and 3.5 µM of the most active inhibitor, 0.1, 0.2, 0.3, 0.4 and 0.5 µM of acetylcholine iodide and a fixed AChE concentration (4 mU/mL in 10 mL phosphate buffer) were used in kinetic tests and assessment was resembled enzyme inhibition assay. A 96-Well microplate was loaded with 145 µL of 200 mM phosphate buffer solution, 10 µL of test sample (2, 2.5 and 3.5 µM), 10 µL of ACh enzyme (4 mU/mL) and 80 µL of DTNB and incubated in dark for 5 min at 25 ºC. The enzymatic reaction was initiated by the addition of 15 µL of substrate ATCh (0.1-0.5 mM), which was then incubated for 5 min. Kinetic characterization was done spectrometrically using a Bio-Rad Elisa microplate reader at 415 nm [20,22]. Each time, a control assay was performed without the test compound. The Lineweaver-Burk plots were created using GraphPad Prism 8. The slopes and intercepts of the double reciprocal plots were plotted against the inhibitor concentrations in order to determine the inhibitor constants (K_{i1} and K_{i2}) associated with the binding of the inhibitor to the free enzyme and the enzyme-substrate complex as intercepts on the negative x-axis. Microsoft Excel was used for data analysis.

ABTS radical scavenging assay: The antioxidant ability of the compounds was evaluated using 2,2′-azino-*bis*(3-ethylbenzothiazoline-6-sulfonic acid) (ABTS) radical scavenging assay. The ABTS radical cation, referred to as $ABTS^{\bullet+}$, was generated by mixing equal volumes of 3 mM potassium persulfate and ABTS stock solution and placing in the dark at room temperature for 12-18 h. Before beginning the experiment, the work solution of $ABTS^{\bullet+}$ was freshly prepared by adding methanol in a ratio of 1:29. After loading the assay mixture composed of 10 µL test solution and 290 µL $ABTS^{\bullet+}$ work solution, the 96-well microplate was then incubated for 30 min, plate was then inserted into the Bio-Rad Elisa reader and the absorbance was determined at 734 nm. The parallel control assay without test compound was carried out. The standard utilized was Trolox. A blank was done in each of the assays using phosphate buffer rather than test compound and Trolox. The IC_{50} values were obtained by doing each assay three times, averaging the results and reporting them as mean ± SEM [23].

Molecular docking studies: Docking studies were conducted using the Molecular Operating Environment (MOE) software package (2015) to explore the interactions of synthesized thiophene piperazine-carbamate derivatives with *Electrophorus electricus* acetylcholinesterase (PDB ID: 1C2O), obtained from the Protein Data Bank (https://www.rcsb.org/). The compounds were first sketched using ChemDraw and then imported into MOE, where they underwent 3D protonation and energy minimization with a 0.01 gradient. The optimized structures were saved as MDB files for subsequent docking calculations. The protein structure was also imported into MOE and the structure preparation wizard was used to correct any issues with the model. Hydrogen atoms were added in standard geometry, solvent molecules were removed and the structure was minimized to achieve the final optimized protein structure, which was saved for the docking process. In the docking setup, dummy atoms were designated as the docking site and the triangle matcher method was chosen for ligand placement. The London dG scoring function was used to evaluate the initial docking poses, followed by rigid receptor refinement. The final selection of the best binding poses was based on the GBVI/WSA dG scoring method. The default values were applied to all scoring methods. The MDB files for the synthesized thiophene piperazine-carbamate derivatives were then loaded into the system and general docking calculations were run automatically. After the docking simulations were completed, the resulting poses were thoroughly analyzed to assess the binding interactions between the ligands and the acetylcholinesterase enzyme [24,25].

RESULTS AND DISCUSSION

The synthesis of thiophene piperazine-carbamate hybrids (**8a-g**) follows a multistep synthetic route. It starts with the nitration of difluorobenzene using a concentrated HNO_3 and H_2SO_4 mixture, yielding 3,4-difluoronitrobenzene (**1**). This intermediate then undergoes nucleophilic substitution with piperazine yielded **2** which is followed by Boc protection to form intermediate **3**. The nitro group of intermediate **3** is subsequently reduced by $NaBH_4$ to give corresponding amine **4**. In the next step, compound **4** undergoes amide bond formation with thiophene-2-carboxylic acid in the presence of EDC·HCl and HOBt, yielding amide **5**. The Boc group in **5** was removed using TFA in DCM, resulting an intermediate **6**. Finally, intermediate **6** was treated with various substituted chloroformates (**7a-g**) under mild conditions, yielding the thiophene piperazine-carbamate hybrids (**8a-g**).

Biological activities

AChE and BChE inhibition activity

AChE inhibition activity: All the synthesized thiophene piperazine-carbamate hybrids (**8a-g**), along with galantamine

as a standard, were assessed for their AChE inhibitory activity, showing notable inhibition with IC_{50} values ranging from 0.12 ± 0.001 μM to 1.90 ± 0.05 μM (Table-1). Among these, compound **8e** (methyl), exhibited the highest potency, with an IC_{50} of 0.12 ± 0.001 μM, establishing it as the most potent inhibitor in the series. Compounds **8d** (ethyl) and **8g** (phenyl) displayed slightly reduced activity, with IC_{50} values of 0.16 ± 0.001 μM and 1.00 ± 0.006 μM, respectively. In contrast, **8c** (isobutyl) and **8f** (fluorenylmethyloxy) demonstrated comparatively lower inhibition, with IC_{50} values of 1.58 ± 0.04 μM and 1.90 ± 0.05 μM respectively, yet all the compounds still exhibited notable inhibitory activities, confirming their effectiveness, albeit with a slight reduction in potency relative to the others.

The SAR study revealed that as alkyl chain length increased, AChE inhibitory activity decreased. Compound **8e** (methyl) exhibited the highest potency, while compounds with longer alkyl chains, such as **8d** (ethyl, IC_{50} = 0.16 ± 0.001 μM) and **8a** (pentyl, IC_{50} = 0.28 ± 0.003 μM) showed progressively reduced inhibition. Furthermore, branching within the alkyl chains also led to diminished potency, as observed with **8b** (*tertiary* butyl, IC_{50} = 0.94 ± 0.02 μM) and **8c** (isobutyl, IC_{50} = 1.58 ± 0.04 μM). These trends suggest that longer and branched hybrids reduce AChE activity due to steric hindrance, which prevents optimal binding in the enzyme's active site and impairs binding efficiency. Compound **8g** (phenyl, IC_{50} = 1.00 ± 0.006 μM) showed moderate inhibition, with the phenyl group allowing adequate binding despite its bulk. In contrast, compound **8f** (fluorenylmethyloxy, IC_{50} = 1.90 ± 0.05 μM) exhibited the weakest inhibition, likely due to the steric bulk of the fluorenylmethyloxy group, which hindered proper alignment in the enzyme's active site. Collectively, the synthesized thiophene piperazine-carbamate hybrids (**8a-g**) demonstrated significant AChE inhibitory activity, with compound **8e** showing the highest potency.

BChE inhibition activity: All the synthesized thiophene piperazine-carbamate hybrids (**8a-g**), along with galantamine as a standard, were evaluated for their BChE inhibitory activity, demonstrating significant inhibition with IC_{50} values ranging from 12.29 ± 0.02 μM to 114.84 ± 0.12 μM. Among these, compound **8e** (methyl) exhibited the highest potency, with an IC_{50} of 12.29 ± 0.02 μM, establishing it as the most effective inhibitor in the series. Compounds **8d** (ethyl) and **8g** (phenyl) showed moderate inhibition, with IC_{50} values of 18.15 ± 0.14 μM and 35.71 ± 0.27 μM, respectively. In contrast, **8a** (pentyl), **8b** (*tertiary* butyl), **8c** (isobutyl) and **8f** (fluorenylmethyloxy) demonstrated comparatively lower inhibition, with IC_{50} values ranging from 42.81 ± 0.24 μM to 114.84 ± 0.12 μM, yet all compounds still exhibited notable inhibitory activities, confirming their effectiveness, albeit with reduced potency relative to the most potent derivatives.

The SAR analysis revealed that shorter alkyl chains and minimal branching enhanced BChE inhibitory activity. Compound **8e** (methyl) showed the highest potency, while compounds with longer alkyl chains, such as **8d** (ethyl, IC_{50} = 18.15 ± 0.14 μM) and **8a** (pentyl, IC_{50} = 107.45 ± 0.02 μM), exhibited progressively reduced inhibition. This suggests that while longer alkyl chains may still provide some inhibition, they introduce steric hindrance, which reduces binding efficiency. Furthermore, branching in the alkyl chains, as seen with compounds **8b** (*tertiary* butyl, IC_{50} = 114.84 ± 0.12 μM) and **8c** (isobutyl, IC_{50} = 106.07 ± 0.04 μM), led to further diminished potency, likely due to steric bulk hindering optimal binding in the enzyme's active site. The presence of aromatic groups also influenced BChE inhibition. Compound **8g** (phenyl, IC_{50} = 35.71 ± 0.27 μM) showed moderate inhibition, with the phenyl group facilitating adequate binding despite its bulk. In contrast, compound **8f** (fluorenylmethyloxy, IC_{50} = 42.81 ± 0.24 μM) demonstrated the weakest inhibition, likely due to the steric hindrance of the fluorenylmethyloxy group, which obstructed proper alignment within the enzyme's active site. In summary, the synthesized thiophene piperazine-carbamate hybrids (**8a-g**) demonstrated variable but significant BChE inhibitory activity, with compound **8e** showing the highest potency.

Selectivity index: The most potent compounds in both AChE and BChE assays are compound **8e** and compound **8d**. Compound **8e** demonstrated the highest potency in AChE inhibition with an IC_{50} of 0.12 ± 0.001 μM and BChE inhibition with an IC_{50} of 12.29 ± 0.02 μM. Its selectivity index (SI) for AChE over BChE is 102.41, indicating a strong preference for inhibiting AChE. Compound **8d** also showed potent inhibition with an AChE IC_{50} of 0.16 ± 0.001 μM and a BChE IC_{50} of 18.15 ± 0.14 μM, with a SI of 113.43, demonstrating a slightly higher selectivity for AChE compared to **8e**. Both compounds exhibit high selectivity for AChE inhibition, highlighting their potential for targeted therapeutic applications in neurodegenerative diseases such as Alzheimer's disease.

TABLE-1
AChE AND BChE INHIBITION AND ABTS RADICAL SCAVENGING ACTIVITIES OF THIOPHENE PIPERAZINE-CARBAMATE HYBRIDS (**8a-g**)

Compounds	IC_{50} (μM) ± S.E.M.		Selectivity for AChE	IC_{50} (μM) ± S.E.M.
	AChE	BChE		ABTS
8a	0.28 ± 0.003	107.45 ± 0.02	383.75	1.089 ± 0.022
8b	0.94 ± 0.02	114.84 ± 0.12	122.17	1.157 ± 0.012
8c	1.58 ± 0.04	106.07 ± 0.04	67.13	1.619 ± 0.34
8d	0.16 ± 0.001	18.15 ± 0.14	113.43	0.434 ± 0.02
8e	0.12 ± 0.001	12.29 ± 0.02	102.41	0.192 ± 0.001
8f	1.90 ± 0.05	42.81 ± 0.24	22.53	2.487 ± 0.013
8g	1.00 ± 0.006	35.71 ± 0.27	35.71	1.491 ± 0.015
Galantamine	0.01 ± 0.003	2.06 ± 0.03	206	–
Trolox	–	–	–	0.112 ± 0.002

ABTS radical scavenging activity: All the synthesized hybrid compounds **8a-g**, alongside Trolox as a standard, were evaluated for their ABTS radical scavenging abilities, showing notable antioxidant activity, with IC_{50} values ranging from 0.19 ± 0.001 μM to 2.49 ± 0.013 μM. Among these, compound **8e** (methyl) exhibited the highest potency, with an IC_{50} of 0.19 ± 0.001 μM, establishing it as the most effective radical scavenger in the series. Compound **8d** (ethyl) showed slightly reduced activity, with an IC_{50} of 0.43 ± 0.02 μM, but still demonstrated substantial radical scavenging potential. In contrast, compound **8f** (fluorenylmethyloxy) and compound **8c** (isobutyl) exhibited comparatively lower activity, with IC_{50} values of 2.49 ± 0.013 μM and 1.62 ± 0.34 μM, respectively, yet both maintained notable antioxidant activity, confirming their effectiveness despite a slight reduction in potency compared to the others.

The SAR analysis revealed that shorter alkyl chains significantly enhance ABTS radical scavenging activity. Compound **8e** (methyl) emerged as the most potent scavenger, with an IC_{50} of 0.19 ± 0.001 μM. As alkyl chain length increased, the scavenging activity progressively diminished, as seen in **8d** (ethyl, IC_{50} = 0.43 ± 0.02 μM) and **8a** (pentyl, IC_{50} = 1.09 ± 0.022 μM), suggesting that shorter alkyl chains provide more efficient interactions with the ABTS radicals, while longer chains reduce radical scavenging efficiency. Moreover, branching within the alkyl chains further decreased antioxidant activity, as observed with compounds **8b** (*tertiary* butyl, IC_{50} = 1.16 ± 0.012 μM) and **8c** (isobutyl, IC_{50} = 1.62 ± 0.34 μM). The incorporation of aromatic groups also influenced radical scavenging potency. Compound **8g** (phenyl, IC_{50} = 1.49 ± 0.015 μM) demonstrated moderate activity, as phenyl group, though bulkier than alkyl chains, still allowed sufficient interaction with the ABTS radicals. On the other hand, compound **8f** (fluorenylmethyloxy, IC_{50} = 2.49 ± 0.013 μM) exhibited the weakest scavenging activity, likely due to the steric hindrance imposed by the larger fluorenylmethyloxy group, which obstructed optimal interaction with the radicals. Overall, the synthesized hybrid compounds (**8a-g**) displayed significant ABTS radical scavenging activity, with compound **8e** demonstrating the highest potency.

Kinetic study on AChE inhibition: Compound **8e** demonstrates superior potency in inhibiting AChE, BChE and exhibiting antioxidant activity, making it an attractive candidate for further study. Given its outstanding performance in all three assays, we extended our investigation to explore the binding mechanism and inhibition strategy of the compound. Inhibition kinetics of **8e** against AChE was analyzed by assessing enzyme activity at various substrate (ATCh) concentrations (0.1, 0.2, 0.3, 0.4 and 0.5 mM) and inhibitor concentrations (IC_{50} = 2.0, 2.5 and 3.5 μM). A Lineweaver-Burk plot was constructed using the reciprocals of initial velocity and substrate concentration (1/v *vs*. 1/S), revealing a mixed-type inhibition pattern characterized by increasing slopes (decreased V_{max}) and intercepts (higher K_m) as the concentration of **8e** increased (Fig. 2). This indicates that **8e** interacts with both the catalytic active site (CAS) and the peripheral anionic site (PAS) of AChE. The inhibitor constants K_{i1} and K_{i2} were determined to be 0.158 μM and 0.347 μM, respectively, through secondary plots of concentration *versus* slope and intercept. These kinetic findings not only confirm the potent inhibition of AChE by **8e** but also suggest that the compound binds effectively to both key sites (CAS and PAS) within the enzyme. This dual interaction further supports its strong inhibitory activity, providing valuable insights for the design of more effective therapeutics targeting cholinesterases.

Molecular docking analysis: All the synthesized hybrid compounds **8a-g** exhibited strong activity in AChE, BChE and ABTS assays, with compound **8e** demonstrating the highest potency across these tests (Table-2). To investigate the mechanisms behind their biological activities, molecular docking studies focused on key regions of the AChE enzyme, including the catalytic active site (CAS), peripheral anionic site (PAS), catalytic radius and mid-gorge regions, which are crucial for enzyme-substrate and enzyme-inhibitor interactions.

Compound **8e**, with a binding energy of -7.50 kcal/mol and an RMSD of 3.31 Å, showed the most efficient binding by interacting with SER203 and HIS447 in the CAS, with minimal steric hindrance from its methyl group, contributing to its high potency. Compound **8b** (binding energy -8.29 kcal/mol, RMSD 1.54 Å) exhibited strong binding, but the bulky *tertiary* butyl group induced steric hindrance, reducing its inhibitory activity. Similarly, compound **8a** (binding energy -8.11 kcal/mol, RMSD 1.89 Å), despite stable binding, suffered from steric clashes due to its pentyl group, limiting its fit and reducing potency. Compound **8c** (binding energy -7.27 kcal/mol, RMSD 1.31 Å) showed good binding at SER203 and TRP86, but the isobutyl group caused steric clashes, reducing its effectiveness. Compound **8d** (binding energy -6.91 kcal/mol, RMSD 1.25 Å) had a slightly lower binding energy but interacted effectively with GLU202 and TYR337 in the CAS and mid-gorge region. However, the longer ethyl group caused some steric hindrance, limiting its overall potency. Compounds **8f** (binding energy -8.42 kcal/mol, RMSD 2.12 Å) and **8g** (binding energy -7.50 kcal/mol, RMSD 1.74 Å) exhibited strong binding but faced steric interference from the larger functional groups (fluorenylmethyloxy in **8f** and bulky groups in **8g**), which diminished their inhibitory potency. In conclusion, while several compounds exhibited high binding energies and favourable docking parameters, **8e** outperformed due to its optimal binding fit, which minimized steric hindrance and enabled more effective enzyme inhibition (Fig. 3).

Conclusion

The synthesized thiophene piperazine-carbamate hybrids (**8a-g**) exhibited promising multi-target activity, effectively inhibiting AChE and BChE while also demonstrating strong antioxidant properties. Among these, compound **8e**, featuring a methyl group, emerged as the most potent, showing superior AChE and BChE inhibition as well as excellent antioxidant activity. The kinetic studies revealed that **8e** exhibited mixed-type inhibition against AChE, interacting with both the CAS and PAS, which was substantiated by the molecular docking studies. The results showed that **8e** formed optimal interactions with key residues in both sites, with a well-fitted structure explaining its superior potency. In contrast, compounds like **8d** (ethyl) and **8g** (phenyl), although potent, exhibited slightly reduced activity, likely due to steric hindrance from their longer

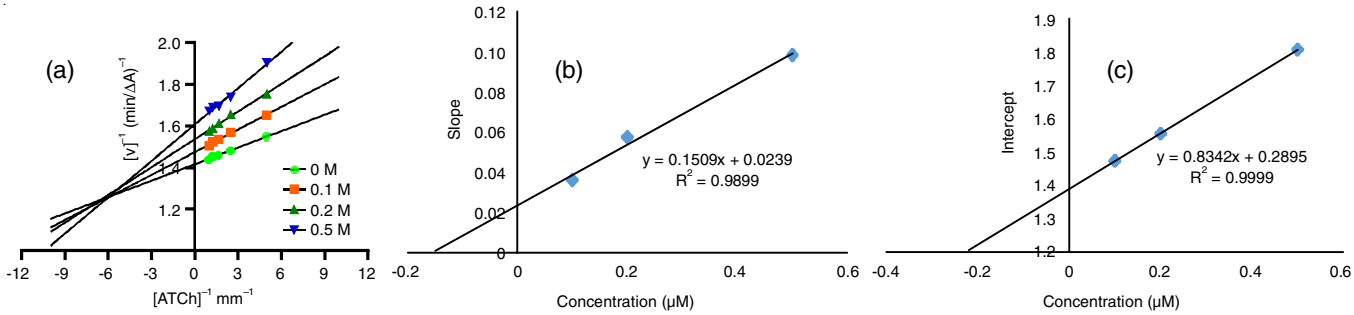

Fig. 2. Kinetics of AChE inhibition for compound **8e**; (a) Lineweaver Burk plot for **8e** (b) Secondary plots of slope and various concentrations of **8e** (c) Intercept and various concentrations of **8e**

TABLE-2
THE BINDING SCORES, RMSD VALUES, LIGAND, RECEPTOR, INTERACTIONS, BINDING SITES DISTANCES AND ENERGY FOR THE THIOPHENE PIPERAZINE-CARBAMATE HYBRIDS (**8a-g**)

Compound	Score (Kcal/mol)	RMSD	Receptor		Interactions	Binding site
8a	-8.11	1.89	SER	293 (B)	π-H	3.84
8b	-8.29	1.54	SER	203 (B)	H-acceptor	3.10
			PHE	295 (B)	H-acceptor	2.88
			HIS	447 (B)	π-H	3.95
8c	-7.27	1.31	SER	203 (B)	H-acceptor	2.80
			TRP	86 (B)	H-π	3.54
			TRP	286 (B)	π-π	3.93
8d	-6.91	1.25	GLU	202 (B)	H-donor	3.21
			TYR	337 (B)	H-π	4.46
8e	-7.50	3.31	SER	203 (B)	H-acceptor	3.05
			HIS	447 (B)	π-H	3.85
			TRP	286 (B)	H-acceptor	2.88
8f	-8.42	2.12	SER	203 (B)	H-acceptor	3.03
			HIS	447 (B)	π-H	3.85
8g	-7.50	1.74	GLN	291 (B)	H-donor	3.99
			TRP	286 (B)	H-π	3.58
			TRP	86 (B)	H-π	3.81
Galantamine	-5.82	1.62	TRP	86 (B)	H-π	3.78

or bulkier groups, as confirmed by docking data. The SAR studies further emphasized that shorter alkyl chain such as the one in **8e**, facilitated more efficient binding and dual inhibition, while longer and branched chains, as seen in compounds **8a** (pentyl) and **8b** (*tertiary* butyl) respectively, caused steric clashes that reduced potency. These findings, drawn from biological assays, kinetics and docking studies, highlight the potential of compound **8e** as a potent multi-target agent, addressing both cholinergic dysfunction and oxidative stress in Alzheimer's disease therapy, making it the most promising candidate for further development.

ACKNOWLEDGEMENTS

The authors express their gratitude to the Department of Bioorganic Chemistry, Yogi Vemana University, Kadapa, India for supporting *in vitro* studies. The authors also express their gratitude to Department of Chemistry, University of Hyderabad, for providing the molecular docking study.

CONFLICT OF INTEREST

The authors declare that there is no conflict of interests regarding the publication of this article.

REFERENCES

1. D.S. Knopman, H. Amieva, R.C. Petersen, G. Chételat, D.M. Holtzman, B.T. Hyman, R.A. Nixon and D.T. Jones, *Nat. Rev. Dis. Primers*, **7**, 33 (2021); https://doi.org/10.1038/s41572-021-00269-y
2. L.K. Huang, Y.C. Kuan, H.W. Lin and C.-J. Hu, *J. Biomed. Sci.*, **30**, 83 (2023); https://doi.org/10.1186/s12929-023-00976-6
3. J. Zhang, Y. Zhang, J. Wang, Y. Xia, J. Zhang and L. Chen, *Signal Transduct. Target. Ther.*, **9**, 211 (2024); https://doi.org/10.1038/s41392-024-01911-3
4. G. Marucci, M. Buccioni, D. Dal Ben, C. Lambertucci, R. Volpini and F. Amenta, *Neuropharmacology.*, **190**, 108352 (2021); https://doi.org/10.1016/j.neuropharm.2020.108352
5. E. Abdallah and R. Abdallah, *RSC Adv.*, **14**, 11057 (2024); https://doi.org/10.1039/D3RA08333K
6. M. Ogos, D. Stary and M. Bajda, *Int. J. Mol. Sci.*, **26**, 157 (2024); https://doi.org/10.3390/ijms26010157
7. E. Tönnies and E. Trushina, *J. Alzheimers Dis.*, **57**, 1105 (2017); https://doi.org/10.3233/JAD-161088
8. K.Y. Yelamanda Rao, S. Jeelan Basha, K. Monika, G. Naidu, I. Sivakumar, S. Kumar, R. Vadde, B.M.R. Aramati, R. Subramanyam and A.G. Damu, *J. Biomol. Struct. Dyn.*, **41**, 11148 (2023); https://doi.org/10.1080/07391102.2023.2203255
9. K. Yelamanda Rao, R. Chandran, K.V. Dileep, S.C. Gorantla, S. Jeelan Basha, S. Mothukuru, I. Siva kumar, K. Vamsi, S. Kumar, A.B.M. Reddy, R. Subramanyam and A.G. Damu, *ACS Chem. Neurosci.*, **15**, 3401 (2024); https://doi.org/10.1021/acschemneuro.4c00424

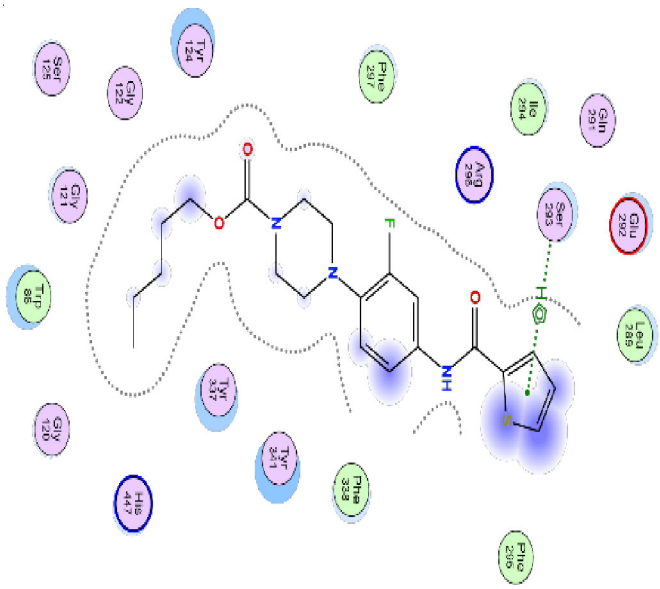
Ser 125
Tyr 124
Gly 122
Phe 297
Ile 294
Gln 291
Arg 296
Ser 293
Glu 292
Gly 121
Trp 86
Leu 289
Tyr 337
Gly 120
Tyr 341
Phe 338
His 447
Phe 295

8a

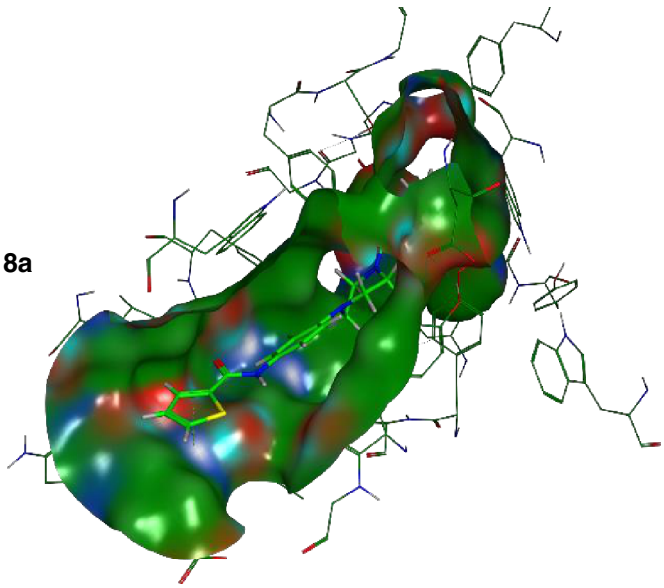

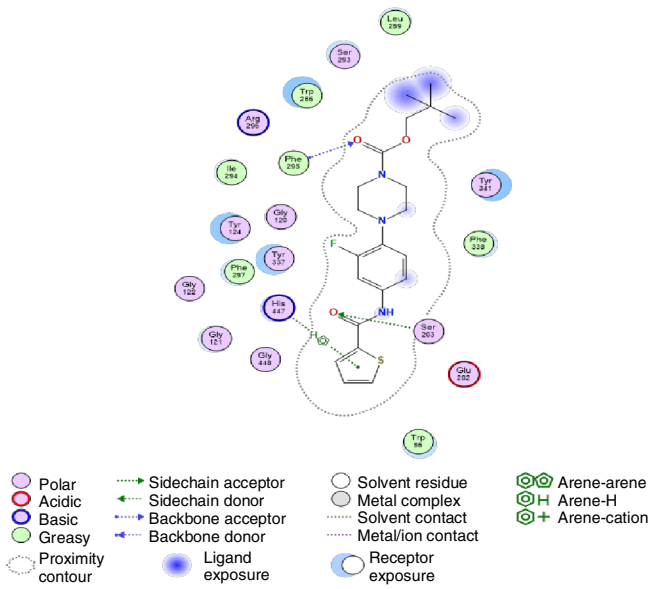
Leu 289
Ser 293
Trp 286
Arg 296
Phe 293
Ile 294
Tyr 337
Gly 120
Tyr 124
Phe 338
Tyr 341
Phe 297
Gly 122
His 447
Ser 203
Gly 121
Gly 448
Glu 202
Trp 86
Polar
Acidic
Basic
Greasy
Proximity contour
Sidechain acceptor
Sidechain donor
Backbone acceptor
Backbone donor
Ligand exposure
Solvent residue
Metal complex
Solvent contact
Metal/ion contact
Receptor exposure
Arene-arene
Arene-H
Arene-cation

8b

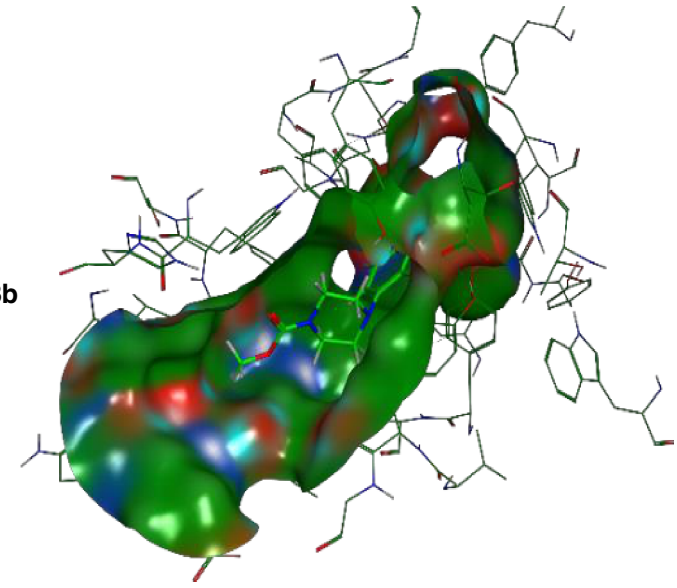

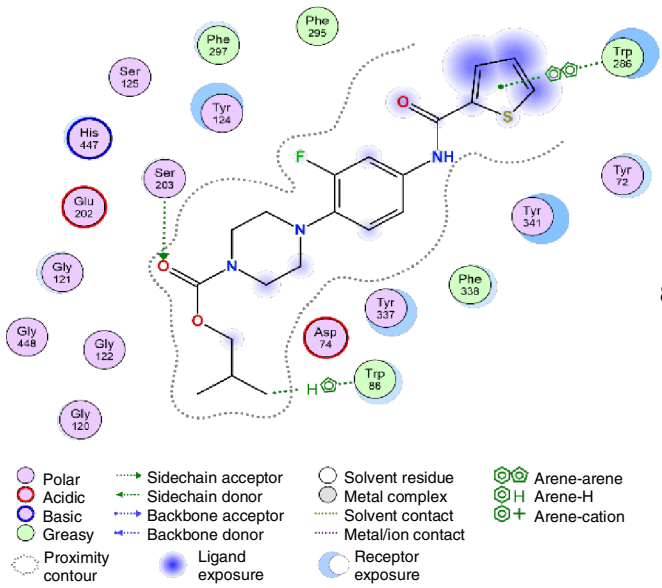
Phe 295
Phe 297
Ser 125
Trp 286
Tyr 124
His 447
Ser 203
Tyr 72
Glu 202
Tyr 341
Gly 121
Phe 338
Tyr 337
Gly 448
Asp 74
Gly 122
Trp 86
Gly 120
Polar
Acidic
Basic
Greasy
Proximity contour
Sidechain acceptor
Sidechain donor
Backbone acceptor
Backbone donor
Ligand exposure
Solvent residue
Metal complex
Solvent contact
Metal/ion contact
Receptor exposure
Arene-arene
Arene-H
Arene-cation

8c

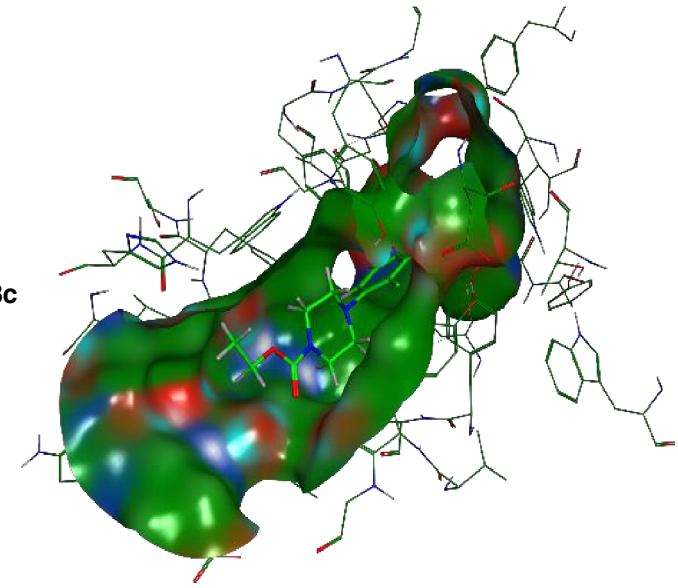

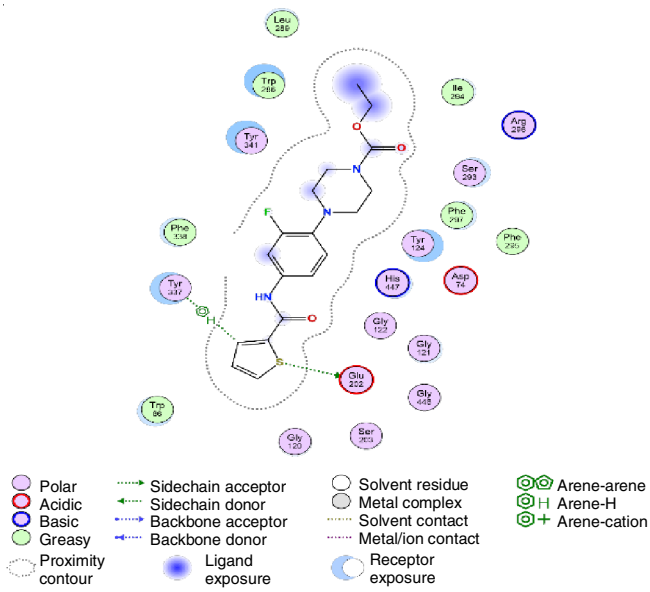
Polar
Acidic
Basic
Greasy
Proximity contour
Sidechain acceptor
Sidechain donor
Backbone acceptor
Backbone donor
Ligand exposure
Solvent residue
Metal complex
Solvent contact
Metal/ion contact
Receptor exposure
Arene-arene
Arene-H
Arene-cation

8d

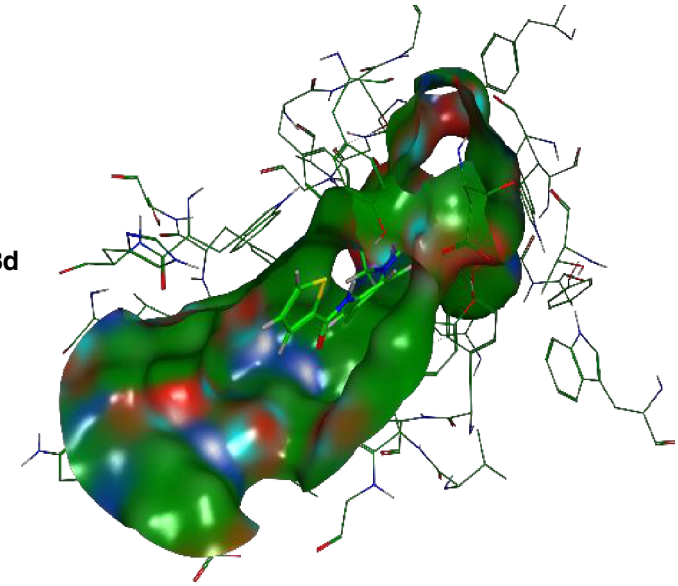

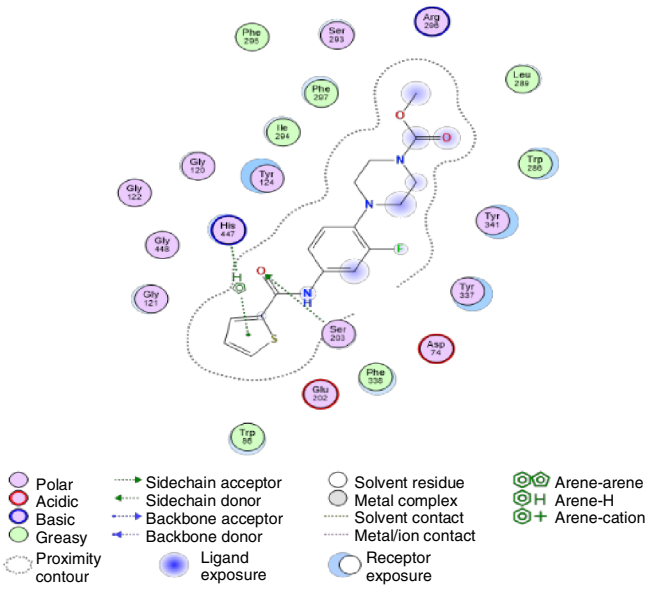
Polar
Acidic
Basic
Greasy
Proximity contour
Sidechain acceptor
Sidechain donor
Backbone acceptor
Backbone donor
Ligand exposure
Solvent residue
Metal complex
Solvent contact
Metal/ion contact
Receptor exposure
Arene-arene
Arene-H
Arene-cation

8e

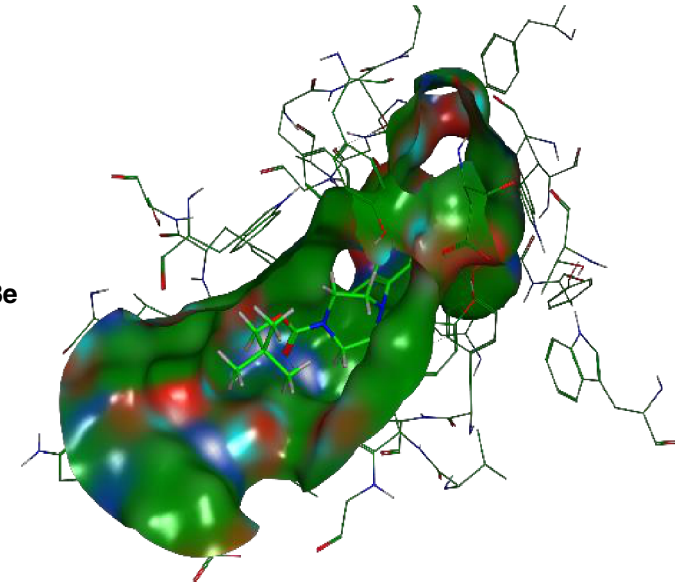

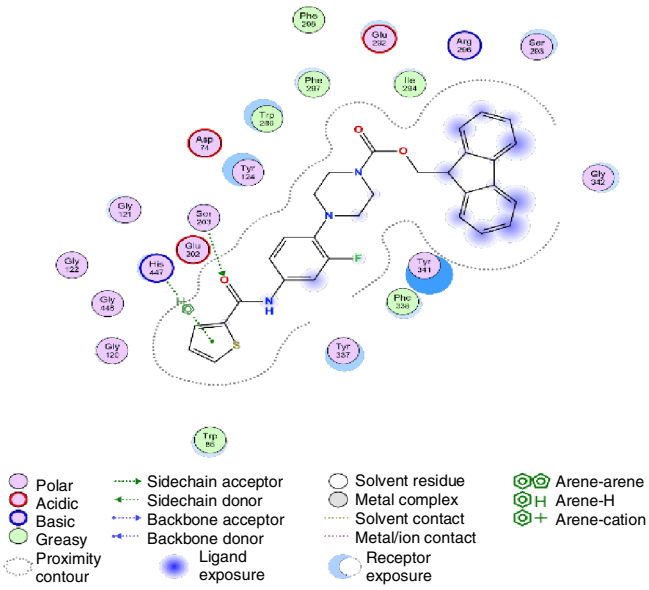
Polar
Acidic
Basic
Greasy
Proximity contour
Sidechain acceptor
Sidechain donor
Backbone acceptor
Backbone donor
Ligand exposure
Solvent residue
Metal complex
Solvent contact
Metal/ion contact
Receptor exposure
Arene-arene
Arene-H
Arene-cation

8f

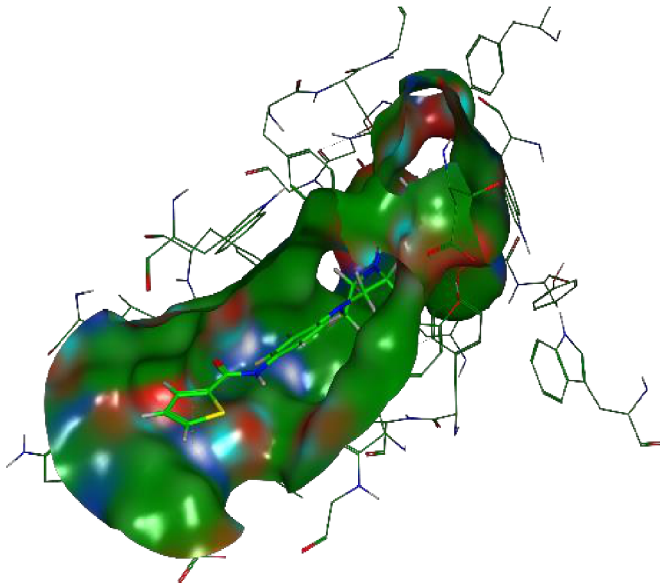

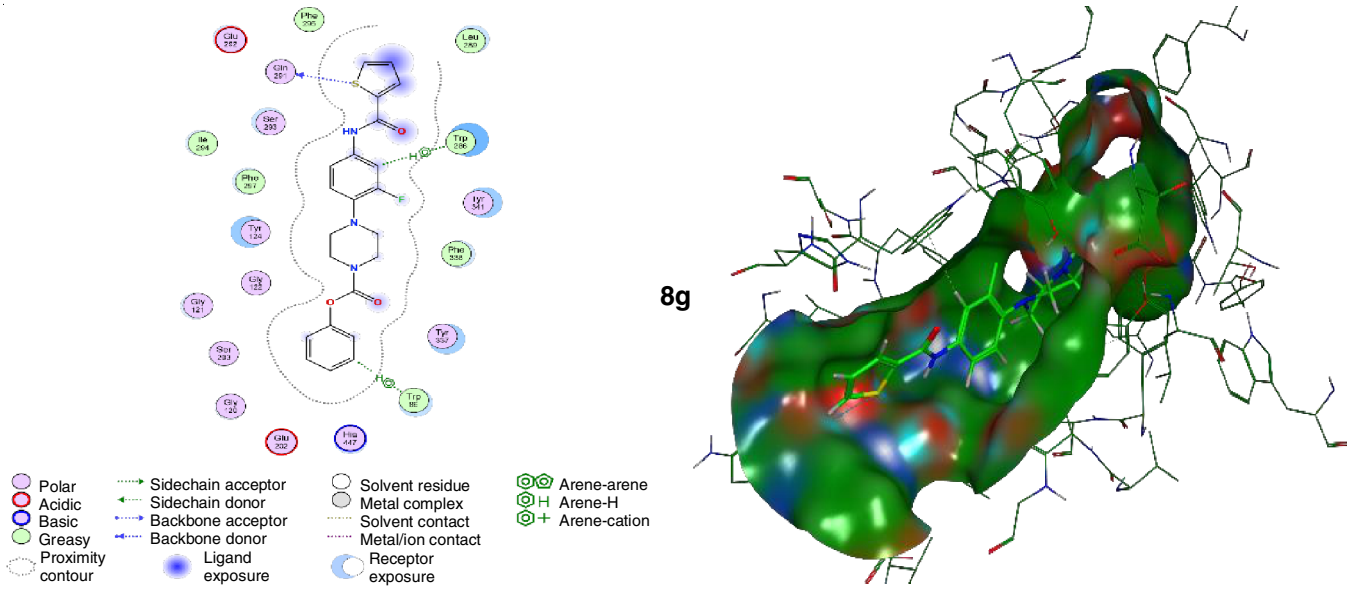

Fig. 3. The 2D & 3D binding modes of **8a**, **8b**, **8c**, **8d**, **8e**, **8f**, **8g** in the active site of AChE

10. S. Thakur, D. Kumar, S. Jaiswal, K.K. Goel, P. Rawat, V. Srivastava, S. Dhiman, H.R. Jadhav and A.R. Dwivedi, *RSC Med. Chem.*, **16**, 481 (2025); https://doi.org/10.1039/D4MD00450G
11. A.K. Rathi, R. Syed, H.S. Shin and R.V. Patel, *Expert Opin. Ther. Pat.*, **26**, 777 (2016); https://doi.org/10.1080/13543776.2016.1189902
12. A.K. Rathi, R. Syed, H.S. Shin and R.V. Patel, *Expert Opin. Ther. Pat.*, **26**, 777 (2016); https://doi.org/10.1080/13543776.2016.1189902
13. N.C. Desai, Y.M. Rupala, A.G. Khasiya, K.N. Shah, U.P. Pandit and V.M. Khedkar, *J. Heterocycl. Chem.*, **59**, 75 (2022); https://doi.org/10.1002/jhet.4366
14. M.S. Kumar, V.S. Krishna, D. Sriram and K. Srinivas, *Eur. J. Med. Chem.*, **164**, 171 (2019); https://doi.org/10.1016/j.ejmech.2018.12.043
15. A. Khalaj, M. Nakhjiri, A.S. Negahbani, M. Samadizadeh, L. Firoozpour, S. Rajabalian, N. Samadi, M.A. Faramarzi, N. Adibpour, A. Shafiee and A. Foroumadi, *Eur. J. Med. Chem.*, **46**, 65 (2011); https://doi.org/10.1016/j.ejmech.2010.10.015
16. C. Jasmine, A. Jain and G. Malik, eds.: J. Madan, A. Baldi and M. Chaudhary, Carbamate–Drug Conjugates in Drug Delivery: Structural and Mechanistic Considerations, In: Polymer-Drug Conjugates, Linker Chemistry, Protocols and Applications, Academic Press, pp. 225-243 (2023); https://doi.org/10.1016/B978-0-323-91663-9.00001-1
17. H. Zhang, Y. Wang, Y. Wang, X. Li, S. Wang and Z. Wang, *Eur. J. Med. Chem.*, **240**, 114606 (2022); https://doi.org/10.1016/j.ejmech.2022.114606
18. Y.P. Singh, N. Kumar, B.S. Chauhan and P. Garg, *Drug Dev. Res.*, **84**, 1624 (2023); https://doi.org/10.1002/ddr.22113
19. M. Vatturu, K.Y. Rao, V.B. Yesu, S.J. Basha, T.P. Guptha, D.S. Babu, K. Sajitha, G.P. Kalyan, A.G. Damu and D. Srinivasulu, *Future Med. Chem.*, **14**, 1741 (2022); https://doi.org/10.4155/fmc-2022-0200
20. K.Y. Yelamanda Rao, S.J. Jeelan Basha, K. Monika, M. Sreelakshmi, I. Sivakumar, G. Mallikarjuna, R.M. Yadav, S. Kumar, R. Subramanyam and A.G. Damu, *Eur. J. Med. Chem.*, **253**, 115288 (2023); https://doi.org/10.1016/j.ejmech.2023.115288
21. G.L. Ellman, K.D. Courtney, V. Andres Jr. and R.M. Featherstone, *Biochem. Pharmacol.*, **7**, 88 (1961); https://doi.org/10.1016/0006-2952(61)90145-9
22. M.V.K. Reddy, K.Y. Rao, G. Anusha, G.M. Kumar, A.G. Damu, K.R. Reddy, N.P. Shetti, T.M. Aminabhavi and P.V.G. Reddy, *Environ. Res.*, **199**, 111320 (2021); https://doi.org/10.1016/j.envres.2021.111320
23. S.S. Dappula, Y.R. Kandrakonda, J.B. Shaik, S.L. Mothukuru, V.R. Lebaka, M. Mannarapu and G.D. Amooru, *J. Mol. Struct.*, **1273**, 134264 (2023); https://doi.org/10.1016/j.molstruc.2022.134264
24. K. Sajitha, V.V.P.C. Narayana, V.B. Yesu, D.M. Manjunath, P.S. Yadav, K. Vamsi, D.S. Babu, V. Murali, A.M. Uttam, A. Anitha, J.B. Prasad, M.C. Subhash, D. Srinivasulu and N.V.V. Jyothi, *Asian J. Chem.*, **37**, 166 (2024); https://doi.org/10.14233/ajchem.2025.32973
25. R.T. Kareem, F. Abedinifar, E.A. Mahmood, A.G. Ebadi, F. Rajabi and E. Vessally, *RSC Adv.*, **11**, 30781 (2021); https://doi.org/10.1039/D1RA03718H